Int J Adv Manuf Technol (2014) 72:1705–1716
DOI 10.1007/s00170-014-5799-2

ORIGINAL ARTICLE

Statistical modelling of weld bead geometry in oscillating arc narrow gap all-position GMA welding

W. H. Xu · S. B. Lin · C. L. Fan · X. Q. Zhuo · C. L. Yang

Received: 17 October 2013 / Accepted: 17 March 2014 / Published online: 2 April 2014

Abstract In this work, the oscillating arc narrow gap all-position gas metal arc (GMA) welding process was developed to improve efficiency and quality in the welding of thick-walled pipes. The statistical models of narrow gap all-position GMA weld bead geometry were developed using response surface methodology (RSM) based on central composite design (CCD). The developed models were checked for their adequacy and significance by ANOVA, and the effects of wire feed rate, travel speed, dwell time, oscillating amplitude and welding position on weld bead dimension were studied. Finally, the optimal welding parameters at welding positions of 0° to 180° were obtained by numerical optimization using RSM.

Keywords Narrow gap welding · All-position welding · GMA welding · Weld bead geometry · CCD · RSM

1 Introduction

Heavy and extra heavy plates are widely used in the ship building industry, pressure vessel, pipeline engineering and ocean engineering. Since it is very difficult or even impossible to change a welding position in such large structures, the all-position gas metal arc (GMA) welding process needs to be used because of its considerable flexibility and productivity [1]. Narrow gap GMA welding (NG-GMAW) is a promising welding process with the advantages of less material consumption, higher efficiency, lower thermal stress and less deformation in welding heavy plates compared with traditional GMA welding [2, 3]. The study on novel narrow gap GMA welding technology for all-position welding is able to promote the development of welding technology in large metal structures.

In all-position GMA welding, the control of the molten pool is a challenge due to liquid metal that is apt to flow down under the action of gravity. Many efforts has been made to solve this problem, which include applying pulse current power to decrease heat input, oscillating arc [4], employing Lorenz force [5] against the gravity of the molten pool. Additionally, NG-GMAW has a high tendency of incomplete sidewall fusion and slag inclusion [6]. Several methods such as rotating arc [3, 7], oscillating arc [8] and twin-wire GMAW [9, 10] were developed to ensure the sufficient penetration of sidewall in NG-GMAW. According to the previous reports, the oscillating arc method is applied not only in all-position welding but also in NG-GMAW. Since the oscillating arc could reduce heat input due to the increase of instantaneous velocity, it is beneficial for the control of the molten pool. Furthermore, the oscillating arc could increase sidewall penetration with increasing heat input of the sidewall. Therefore, in this paper, the oscillating arc narrow gap all-position GMA welding process is proposed.

In order to ensure weld quality, the oscillating arc narrow gap all-position GMAW process must be employed in automatic mode in an industry. In such applications, the selection of optimal weld parameters and control of weld bead shape has become essential because it has a significant effect on mechanical strength of welded joints. In oscillating arc all-position NG-GMAW, the weld bead shape is affected not only by weld parameters such as weld current and weld speed, but also by weld position and arc oscillation parameters such as oscillating amplitude and dwell time. So, it is very difficult to fix several optimal parameters to get the desired weld bead shape. To achieve this objective, the interrelationship between weld bead geometry and weld parameters requires to be developed. Many efforts have been made to develop statistical models to study this relationship and optimize parameters [11, 12]. Gunaraj et al [13] optimized the SAW parameters by

W. H. Xu · S. B. Lin (✉) · C. L. Fan · X. Q. Zhuo · C. L. Yang
State Key Laboratory of Advanced Welding and Joining, Harbin Institute of Technology, Harbin 150001, People's Republic of China
e-mail: sblin@hit.edu.cn

using response surface methodology (RSM); regression models were developed to predict weld bead geometric parameters. Koleva [14] studied the relationship between electron beam welding parameters and weld bead shape, and statistical modelling was developed to optimize the parameters. Starling et al [15] studied the effects of the welding parameters on the weld bead shape in a narrow gap TIG welding process with magnetic arc oscillation by employing a statistical experimental design method, and linear regression equations were developed. Kim et al [16] developed an empirical model for back-bead geometry in root-pass welding of a pipeline. Badkar et al [17] applied the RSM and central composite design (CCD) to develop a model for laser-herded bead profile and optimized the laser-transformations hardening parameters. The geometry model was developed at a certain position in the early reports, but in oscillating arc all-position narrow gap GMA welding, the welding position should be one of the input parameters of the geometry model due to each weld bead consists of flat, vertical and overhead positions [18].

The main purpose of this research is to develop a novel oscillating arc narrow gap all-position GMA welding process and a statistical model of weld bead shape using RSM based on CCD.

2 Experimental apparatus and procedure

The schematic diagram of oscillating arc narrow gap GMA welding torch is shown in Fig. 1. The lower part of the conducting rod is bent to form an angle of 7°, while the upper part makes contact with the carbon brush which is connected

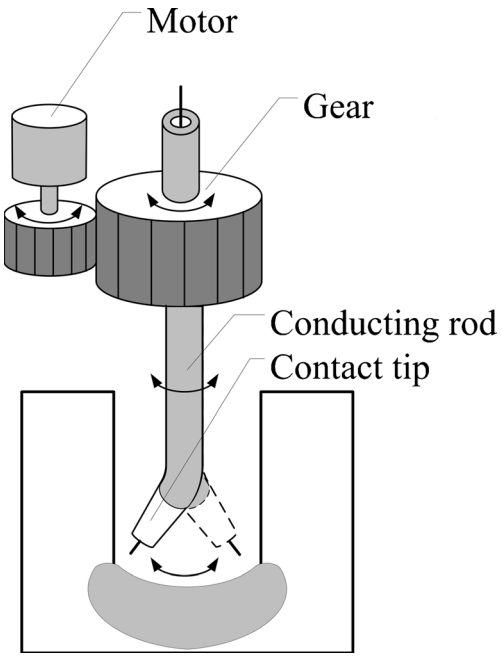

Fig. 1 Schematic diagram of oscillating arc welding torch

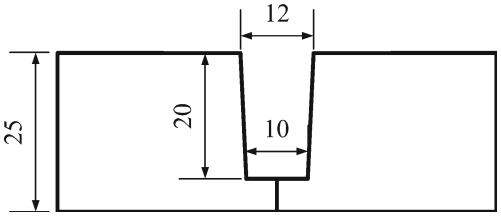

Fig. 2 Schematic diagram of groove size

to the positive terminal of a power source. The electrode wire is fed through the inner hole of the conducting rod and stretches out from the contact tip which is screwed into the lower part of the conducting rod, so there is an angle of 7° between the wire and the axis of the conducting rod. The servo motor rotates the conducting rod and contact tip through a pair of gears, then the arc between the end of the electrode wire and the base metal is driven to oscillate in the narrow gap groove.

In this study, experiments were performed on a plate instead of a pipe. The base material was low carbon steel plates of 25 mm in thickness which were employed to prepare the narrow gap groove. The schematic diagram of the narrow gap groove is shown in Fig. 2.

The filler wire is ER50-6 with a 1.2-mm diameter. The chemical compositions of the base metal and the filler wire are listed in Table 1. Ar (92 %) + CO_2 (8 %) mixture gas is selected as a shielding gas, and the gas flow rate is 15 L min^{-1} during welding.

Three transverse sections were cut from each weld plate. These specimens were ground with grinding papers and polished. Then, the samples were etched in saturated ferric chloride solution. The profiles of the beads were traced by the optical microscope OLYMPUS SZX12. The high-accuracy measurement software analySIS FIVE supplied by OLYMPUS Corporation was used to measure weld dimensions in magnified tracings. In order to reduce the measurement error, each measurement was repeated for three times, and the final result was the average of the three measurements. The experiment results show that the measurement error is ±0.01 mm.

In this paper, a five-level CCD with full replication was applied to a design experimental, and the design software Design-Expert V8.0.6 was used to establish the design matrix and analyze the experimental data.

The procedure of this research was as follows:

(a) Selection of the important factors and finding their upper and lower limits

Table 1 Chemical composition of base metal and filler wire (wt%)

	C	Si	S	P	Ni	Cr	Cu	Mn
Base metal	0.16	0.30	0.033	0.035	0.28	0.30	0.30	0.78
Filler wire	0.08	0.10	0.034	0.022	–	–	0.30	1.52

(b) Designing experimental matrix by Design-Expert V8.0.6
(c) Conducting the experiments as the design matrix
(d) Recording the responses parameters
(e) Calculating regression coefficients of input parameters and developing statistical models
(f) Checking the significance of models and regression coefficients
(g) Validation of models
(h) Analysis of results
(i) Optimizing welding parameters

3 Development of statistical modelling

The results of the initial trials show that four weld parameters are the most important factors affecting the weld bead geometry, namely the wire feed rate (W), the travel speed (T), the dwell time (S) and the oscillating amplitude (α). Moreover, the welding position (θ) also affects the weld bead shape significantly. In order to develop statistical models to describe and predict the weld bead shape in all welding positions, W, T, S, α *and* θ were selected as input parameters. The schematic diagrams of oscillating amplitude and welding position are shown in Figs. 3 and 4.

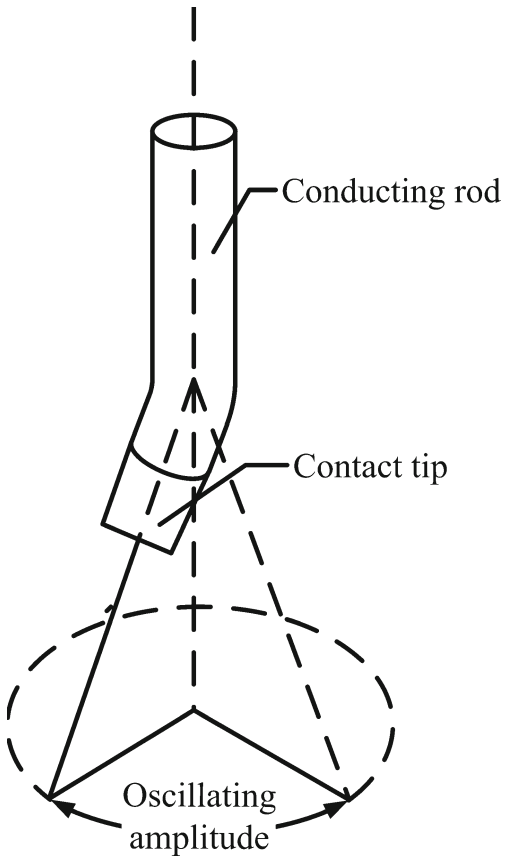

Fig. 3 Schematic diagram of oscillating amplitude

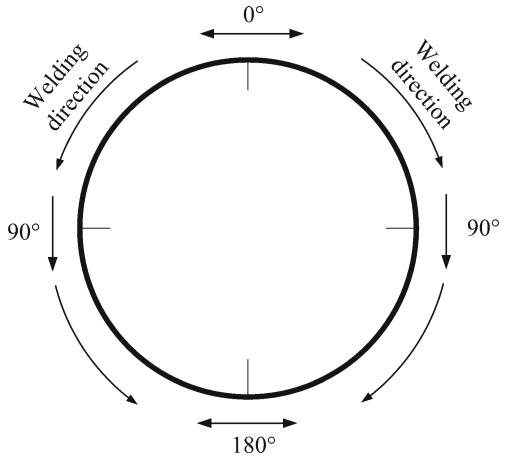

Fig. 4 Schematic diagram of welding position

Trial runs were conducted by varying one of the process parameters at a time while keeping the rest of them at constant value to determine the range of each input parameter. The working range was fixed by the stability of welding process and the absence of visible defects. In order to optimize welding parameters, the CCD should be rotatable due to a rotatable design that can provide equal precision of estimation in all directions. A rotatable CCD means that the variance of the predicted response is the same at all the points which are the same distance from the design centre. A CCD can be made rotatable by the selection of β which is the distance of the axial runs from the design centre. The value of β for rotatable CCD is depended on the number of input parameters; in fact, $\beta=(2^k)^{1/4}$ gets a rotatable CCD where k is the number of input parameters. In this paper, the number of input parameters is 5, so the value of β is $32^{1/4}=2.38$. Therefore, the upper and lower limits of the design were coded as +2.38 and −2.38 respectively. The code values for intermediate values can be calculated by Eq. 1.

$$X_i = \frac{2.38(2X-(X_{\max}+X_{\min}))}{X_{\max}-X_{\min}} \quad (1)$$

where X_i is the required code value of a variable X, and X is any value of the variable from $X_{\min}$ to $X_{\max}$; $X_{\max}$ and $X_{\min}$ are the upper limits and lower limits of the variable X,

Table 2 Coded values and factor levels

Factors	Unit	Coded value				
		−1	1	0	−2.38	2.38
W	m min^{-1}	6.6	7.4	7	6	8
T	mm min^{-1}	269	298	283	250	317
S	ms	158	242	200	100	300
α	°	50	59	55	45	65
θ	°	52	128	90	0	180

Table 3 Central composite design matrix and measured response

Std	Run	Coded variables					Response parameters			
		W	T	S	α	θ	SP (mm)	WP (mm)	C (mm)	WH (mm)
1	25	−1	−1	−1	−1	−1	0.38	1.01	2.58	1.64
2	27	1	−1	−1	−1	−1	0.36	1.36	2.69	2.01
3	29	−1	1	−1	−1	−1	0.28	1.19	2.58	1.33
4	46	1	1	−1	−1	−1	0.38	1.38	2.57	1.64
5	43	−1	−1	1	−1	−1	0.45	0.94	2.80	1.83
6	4	1	−1	1	−1	−1	0.40	1.19	2.74	2.02
7	42	−1	1	1	−1	−1	0.37	1.30	2.15	1.63
8	48	1	1	1	−1	−1	0.47	1.65	3.14	1.52
9	50	−1	−1	−1	1	−1	0.50	1.15	3.27	1.58
10	31	1	−1	−1	1	−1	0.36	1.37	3.00	2.08
11	2	−1	1	−1	1	−1	0.30	1.22	2.80	1.28
12	37	1	1	−1	1	−1	0.38	1.24	2.94	1.59
13	10	−1	−1	1	1	−1	0.41	0.90	2.19	1.82
14	5	1	−1	1	1	−1	0.45	1.34	2.70	1.65
15	20	−1	1	1	1	−1	0.54	1.39	3.02	1.42
16	24	1	1	1	1	−1	0.49	1.51	3.08	1.72
17	35	−1	−1	−1	−1	1	0.20	1.38	1.85	1.85
18	8	1	−1	−1	−1	1	0.33	2.16	2.33	2.05
19	22	−1	1	−1	−1	1	0.35	1.82	2.21	1.69
20	39	1	1	−1	−1	1	0.24	1.98	2.15	1.85
21	49	−1	−1	1	−1	1	0.22	2.33	2.30	1.62
22	13	1	−1	1	−1	1	0.35	2.22	2.82	1.56
23	45	−1	1	1	−1	1	0.19	1.56	2.21	1.55
24	21	1	1	1	−1	1	0.30	2.49	2.45	1.70
25	7	−1	−1	−1	1	1	0.29	1.79	2.56	1.74
26	12	1	−1	−1	1	1	0.19	2.02	2.53	1.92
27	34	−1	1	−1	1	1	0.27	2.03	2.69	1.21
28	18	1	1	−1	1	1	0.29	1.95	2.64	1.70
29	44	−1	−1	1	1	1	0.31	1.72	2.53	1.70
30	30	1	−1	1	1	1	0.45	1.91	3.06	2.22
31	40	−1	1	1	1	1	0.39	1.49	3.71	1.03
32	36	1	1	1	1	1	0.52	2.14	2.66	1.64
33	38	−2.38	0	0	0	0	0.40	1.10	3.73	1.20
34	14	2.38	0	0	0	0	0.64	1.38	4.09	2.21
35	33	0	−2.38	0	0	0	0.39	1.24	2.58	2.06
36	19	0	2.38	0	0	0	0.42	1.18	3.08	1.34
37	47	0	0	−2.38	0	0	0.36	1.21	3.86	1.84
38	15	0	0	2.38	0	0	0.47	1.37	3.25	1.39
39	9	0	0	0	−2.38	0	0.39	1.49	3.20	1.68
40	41	0	0	0	2.38	0	0.51	1.02	5.05	1.70
41	1	0	0	0	0	−2.38	0.45	1.54	1.31	2.40
42	16	0	0	0	0	2.38	0.20	3.04	0.71	3.50
43	6	0	0	0	0	0	0.40	1.49	2.49	1.42
44	28	0	0	0	0	0	0.54	1.26	3.60	1.31
45	11	0	0	0	0	0	0.64	1.40	3.58	1.84
46	26	0	0	0	0	0	0.39	1.27	3.30	1.66
47	32	0	0	0	0	0	0.50	1.34	3.08	1.45

Table 3 (continued)

Std	Run	Coded variables					Response parameters			
		W	*T*	*S*	α	θ	SP (mm)	WP (mm)	C (mm)	WH (mm)
48	3	0	0	0	0	0	0.45	1.31	3.11	1.42
49	17	0	0	0	0	0	0.43	1.16	4.00	1.45
50	23	0	0	0	0	0	0.52	1.61	2.15	1.54

respectively. The factor levels in relation to the coded values are shown in Table 2. The design matrix consisting 50 sets of coded conditions is shown in Table 3.

The experiments were conducted as the design matrix, and the weld bead specimens were prepared as the aforementioned steps to measure the sizes of weld bead geometry. The response parameters namely sidewall penetration (SP), weld penetration (WP), concavity (C) and weld height (WH) were measured. Figure 5 shows the cross section of narrow gap weld bead. The measured responses are shown in Table 3.

According to the central composite design matrix and measured response, the regression model can be developed. The relationship between weld bead geometry and the input parameters could be expressed as $y = F(x_1, x_2, \ldots\ldots, x_i)$, where y is the measured response, and x_i is the input parameter. y_{trans} is a power transformation of y, so the response function selected being a second-order model can be represented as Eq. 2.

$$y_{trans} = b_0 + \sum_{i=1}^{5} b_i x_i + \sum_{i=1}^{4}\sum_{j=i+1}^{5} b_{ij} x_i x_j + \sum_{i=1}^{5} b_{ii} x_i^2 \qquad (2)$$

The values of the regression coefficients could be calculated by the least squares method. Therefore, the regression coefficients of the model of CCD with five factors were calculated by Eqs. 3, 4, 5 and 6

$$b_0 = 0.0987822\sum_{i=1}^{50} y_i - 0.019101\sum_{j=1}^{5}\sum_{i=1}^{50} x_{ij}^2 y_i \qquad (3)$$

$$b_i = 0.02309\sum_{i=1}^{50} x_{ij} y_i \qquad (4)$$

$$b_{ij} = 0.03125\sum_{i=1}^{50} x_{ik} x_{ij} y_i \qquad (5)$$

$$b_{ii} = 0.01562499\sum_{i=1}^{50} x_{ij}^2 y_i + 0.00146131\sum_{j=1}^{5}\sum_{i=1}^{50} x_{ij}^2 y_i - 0.019101\sum_{i=1}^{50} y_1 \qquad (6)$$

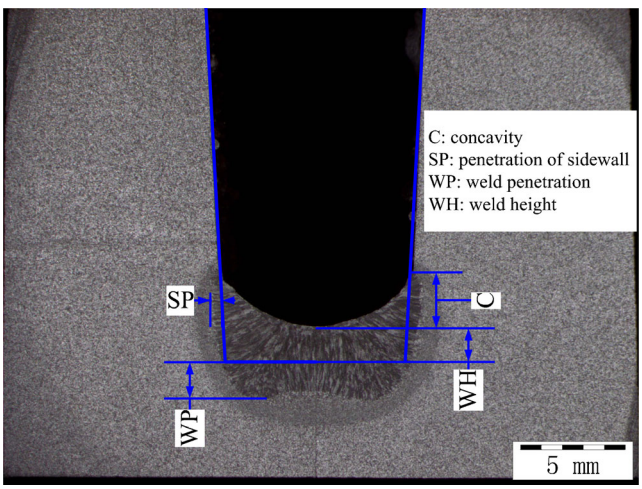

Fig. 5 Weld bead shape measurement definitions

A step-wise regression method which eliminates the insignificant terms automatically was selected to develop the regression models. The adequacy of the models and the significance of regression coefficients were tested by ANOVA technique. The results of ANOVA for models are shown in Tables 4, 5, 6 and 7.

Table 4 shows the result of ANOVA for the SP model; the model F value is $9.3677324 > F_{0.01}(6,43) = 3.29$; the probability of F (prob>F value of model) is less than 0.0001, that is to say the model is significant. The test result of lack-of-fit shows that it is insignificant relative to the pure error; insignificant lack-of-fit indicates the second-order model is adequate. The results of significance test for model terms are also shown in Table 3; when the value of "prob>F" of the model term is less than 0.05, the model term is significant, while the value of prob>F greater than 0.1 indicates the model term is insignificant. According to Table 3, S, α, θ and second order of

Table 4 ANOVA results for penetration of sidewall model

Source	Sum of squares	*df*	Mean square	*F* value	*p* value (prob>*F*)	
Model	2.52	6	0.42	9.37	<0.0001	Significant
W	0.17	1	0.17	3.77	0.059	
S	0.37	1	0.37	8.16	0.007	
α	0.22	1	0.22	4.93	0.032	
θ	1.12	1	1.12	25.05	<0.0001	
$S\times\alpha$	0.15	1	0.15	3.37	0.073	
θ^2	0.49	1	0.49	10.93	0.002	
Residual	1.93	43	0.04			
Lack-of-fit	1.73	36	0.05	1.73	0.231	Not significant
Pure error	0.19	7	0.03			
Cor total	4.44	49				

welding position (θ^2) are the most significant terms of the SP model; two-level interaction of wire feed rate and oscillating amplitude of arc ($W\times\alpha$) also could affect SP.

The results of ANOVA for the WP model, C model and WH model are shown in Tables 5, 6 and 7, respectively. These results show that all the models are significant and adequate. W, θ and θ^2 are the most significant terms of the WP model according to Table 5; two level interaction of travel speed and welding position ($T\times\theta$) is an important term of the model. From Table 6, α, θ, second-order of oscillating amplitude of arc (α^2) and θ^2 are the most significant terms of the concavity model; second-order of wire feed rate (W^2) could affect concavity. The analysis of variance from Table 7 indicates that W, T and θ^2 are the most significant terms in the WH model.

The final statistical models in actual factors are given below:

$$\begin{aligned}\ln(\mathrm{SP}) = {} & 0.82572 + 0.14848W - 0.019182S \\ & - 0.160714\alpha + 0.00725102\theta \\ & + 0.000388475\mathrm{S}\times\alpha \\ & - 0.0000639142\theta^2\end{aligned} \tag{7}$$

$$\begin{aligned}\ln(\mathrm{WP}) = {} & -3.65956 + 0.1985W + 0.00933862T \\ & + 0.016277\theta - 0.0000820542T\times\theta \\ & + 0.0000677208\theta^2\end{aligned} \tag{8}$$

$$\begin{aligned}\ln(\mathrm{C}) = {} & 15.21567 - 2.71098W \\ & - 0.23146\alpha + 0.024969\theta \\ & + 0.01981W^2 + 0.0022677\alpha^2 \\ & - 0.00014892\theta^2\end{aligned} \tag{9}$$

$$\begin{aligned}\ln(WH) = {} & 1.31359 + 0.21404W - 0.00653731T \\ & - 0.012527\theta + 0.0000728821\theta^2\end{aligned} \tag{10}$$

4 Validation of models

In order to ensure the models developed can be applied to predicate and control weld bead geometry in actual application, the accuracy of the models was tested. The test experiments were conducted by assigning different values for input parameters within their working ranges but different from that

Table 5 ANOVA results for weld penetration model

Source	Sum of squares	*df*	Mean square	*F* value	*p* value (prob>*F*)	
Model	2.63	5	0.53	31.42	<0.0001	Significant
W	0.31	1	0.3	18.27	0.0001	
T	0.03	1	0.03	1.94	0.1705	
θ	1.68	1	1.68	100.41	<0.0001	
$T\times\theta$	0.06	1	0.06	3.62	0.0635	
θ^2	0.55	1	0.55	32.84	<0.0001	
Residual	0.74	44	0.02			
Lack-of-fit	0.66	37	0.02	1.68	0.2431	Not significant
Pure error	0.07	7	0.01			
Cor total	3.37	49				

Table 6 ANOVA results for concavity model

Source	Sum of squares	*df*	Mean square	*F* value	*p* value (prob>*F*)	
Model	3.44	6	0.57	28.04	<0.0001	Significant
W	0.03	1	0.03	1.46	0.233	
α	0.25	1	0.25	12.12	0.001	
θ	0.19	1	0.19	9.39	0.004	
W^2	0.07	1	0.07	3.44	0.071	
α^2	0.09	1	0.09	4.50	0.040	
θ^2	2.59	1	2.59	126.73	<0.0001	
Residual	0.88	43	0.02			
Lack-of-fit	0.58	36	0.02	0.38	0.972	Not significant
Pure error	0.30	7	0.04			
Cor total	4.32	49				

of the design matrix. The percentage of errors, predicated response and measured response are shown in Table 8. It is found that the average error for all models is less than 10 %, and all average errors are in the range of engineering errors and accepted in the industry. So, the models can be employed to predicate the weld bead geometry and optimize parameters.

5 Effects of parameters on weld bead shape

Based on the above models, the main and interaction effects of input parameters on weld bead shape can be analyzed.

5.1 Effects of input parameters on SP

Figures 6 and 7 show the effects of wire feed rate and welding position on sidewall penetration, respectively. From Fig. 6, the sidewall penetration is less than 1 mm in the working ranges, and it increases gradually from 0.38 to 0.52 mm with the increase in W from 6 to 8 m min^{-1}. It is due to the increase in input heat of the sidewall.

In Fig. 7, SP increases as θ increases from 0 to 60°, and then it reduces for further increase in θ. SP is maximum when the welding position is 60°. This could be due to the influence of gravity on the molten pool. The component force at the welding direction causes liquid molten metal flowing to the front of the molten pool, and it increases with the increase in θ from 0to 60°. The liquid molten metal at the front of the molten pool is pushed to the sidewall by the arc pressure. The heat input of the sidewall increases as θ increases from 0to 60° due to the increase of the molten liquid at the front molten pool. When θ is more than 90°, the molten liquid at the front molten pool reduces as θ increases due to the reduction of the component force. Otherwise, the closest distance between wire tip and sidewall reduces with the increase of θ from 0 to 60°, due to the increase in the volume of molten liquid at the front molten pool which causes the wire extension reduction; when θ is more than 90°, the closest distance increases as θ increases. SP increases as the closest distance reduces. The mixed trend is attributed to the above reasons.

The interaction of S and α on SP is represented in Fig. 8. SP increases with the increase of S and α at all values. The rate of the increase in SP with the increase in S increases gradually as α increases, and the rate of increase in SP with α increases as S increases. It is due to the fact that all S and α have a positive effect on heat input of the sidewall.

Table 7 ANOVA results for weld height model

Source	Sum of squares	*df*	Mean square	*F* value	*p* value (prob>*F*)	
Model	1.37	4	0.34	25.16	<0.0001	Significant
W	0.35	1	0.35	25.70	<0.0001	
T	0.36	1	0.36	26.67	<0.0001	
θ	0.02	1	0.02	1.59	0.214	
θ^2	0.64	1	0.64	46.67	<0.0001	
Residual	0.61	45	0.01			
Lack-of-fit	0.53	38	0.01	1.24	0.412	Not significant
Pure error	0.08	7	0.01			
Cor total	1.99	49				

Table 8 Comparison of actual and predicated values of the weld bead geometry

	Run	1	2	3	4	5
Input parameters	W (m min^{-1})	6.2	7.2	6.8	7.8	7.5
	T (mm min^{-1})	269	280	290	300	280
	S (ms)	220	250	200	250	100
	α (°)	50	45	65	55	55
	θ (°)	90	52	128	0	180
Predicted values of wed bead shape	SP (mm)	0.33	0.35	0.36	0.45	0.14
	WP (mm)	1.13	1.26	1.74	2.02	4.23
	C (mm)	3.20	2.83	3.46	1.29	0.85
	WH (mm)	1.41	1.77	1.59	2.78	3.30
Actual values of weld bead shape	SP (mm)	0.32	0.36	0.39	0.48	0.13
	WP (mm)	1.21	1.21	1.87	1.92	4.51
	C (mm)	3	2.65	3.23	1.23	0.78
	WH (mm)	1.3	1.89	1.64	2.58	3.25
Percentage error (%)$=100\times\frac{\text{actual value}-\text{predicted value}}{\text{predicted value}}$	SP	−3.03	2.86	8.33	6.67	−7.14
	WP	7.08	−3.97	7.47	−4.95	6.62
	C	−6.25	−6.36	−6.65	−4.65	−8.24
	WH	−7.80	6.78	3.14	−7.19	−1.52

5.2 Effects of input parameters on WP

As shown in Fig. 9, WP increases as W increases from 6 to 8 m min^{-1}. The reason is the liner input increases as the wire feed rate increases due to the increase of a welding current. The interaction of T and θ are represented in Fig. 10. WP increases as T increases when θ is less than 90°, while it decreases as T increases when θ is more than 90°. WP reduces gradually as the increase of θ, and then it increases significantly for further increases in θ. WP is minimum for all values of θ when θ is 45°.

5.3 Effects of input parameters on concavity

Figures 11, 12 and 13 show the effects of W, α and θ on C, respectively. C reduces with the increase of W from 6 to 6.85 m min^{-1}, and then it increases as the further increase in W. This is attributed to the fact that the concavity of a weld bead is affected by the arc force and volume of the molten pool. When W increases, the arc force which results in the increase of C increases due to the increase of the welding current. However, the volume of the molten pool increases as W increases, and it has a negative effect on C. The combined effects of the arc force and molten pool result in the mixed trend.

According to Fig. 12, when α is less than 51°, C reduces gradually as α increases, and then C increases with the further increase in α. As shown in Fig. 13, maximum value of C for all values of θ is obtained when θ is 90°. C increases with the increase in θ from 0 to 90°. When θ is more than 90°, C reduces as θ increases. This is attributed to the fact that liquid molten metal follows below the arc by the effect of molten pool gravity and the arc force makes the molten pool surface depressed.

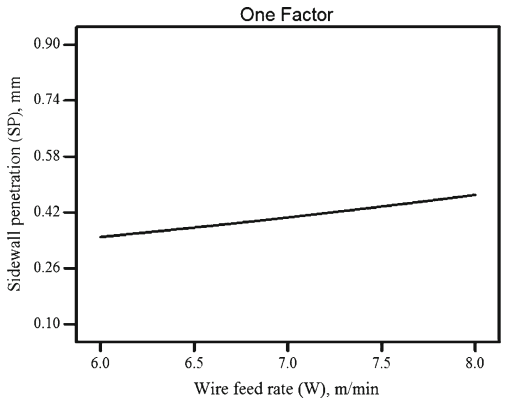

Fig. 6 Direct effect of wire feed rate on sidewall penetration

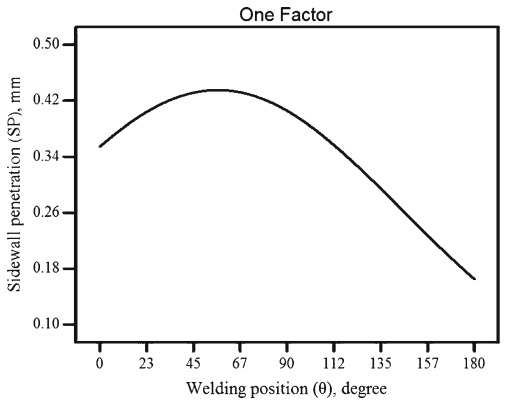

Fig. 7 Direct effect of welding position on sidewall penetration

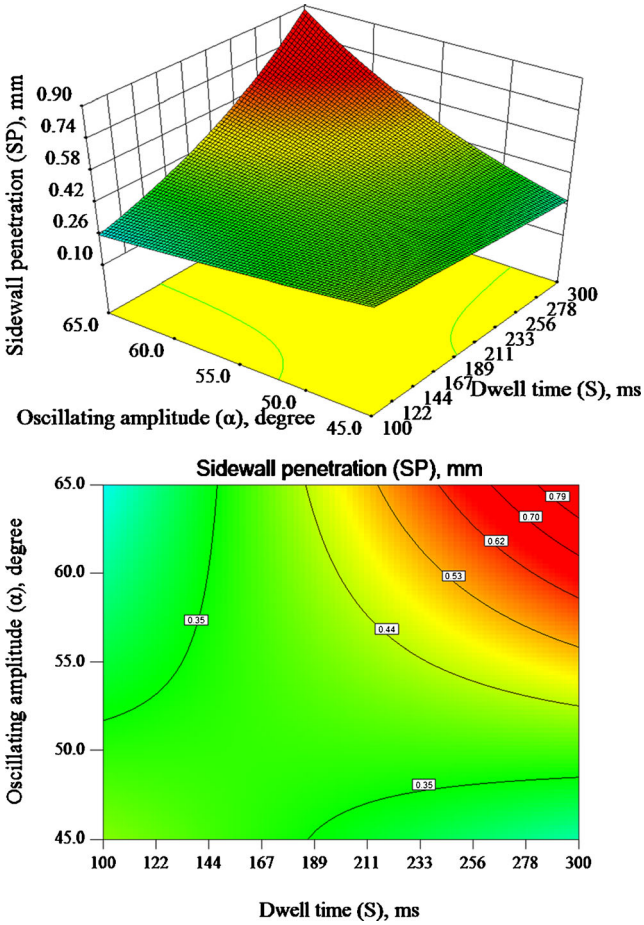

Fig. 8 Interaction of dwell time and oscillating amplitude on sidewall penetration

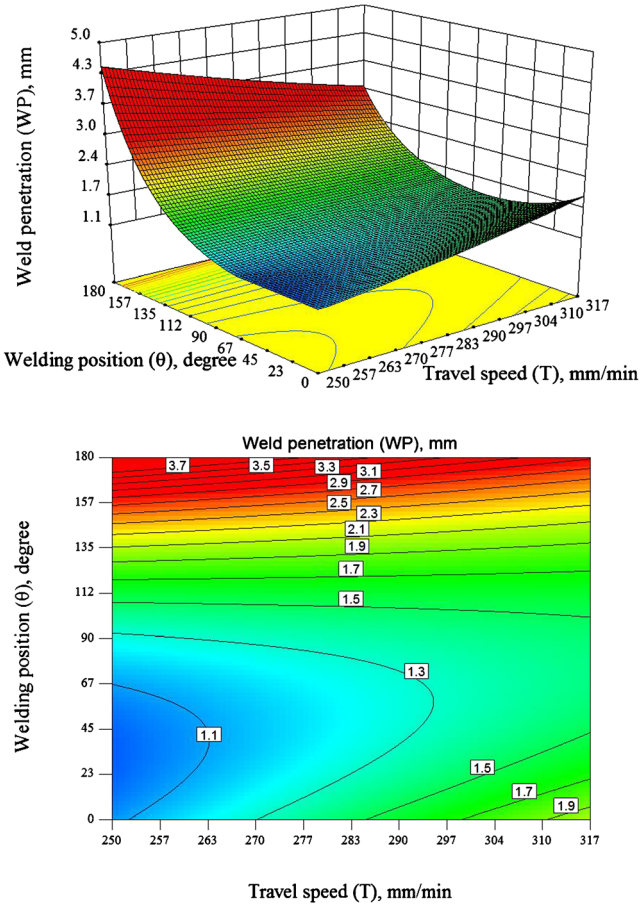

Fig. 10 Interaction of travel speed and welding position on weld penetration

5.4 Effects of input parameters on weld height

Figure 14 shows weld height increases steadily from 1.23 to 1.89 mm with the change of the wire feed rate from 6 to 8 m min^{-1}. Increase in the wire feed rate gives rise to the volume of molten metal at per-unit-length increase, so the weld height increases. Since the increase of travel speed could reduce the volume of the molten metal at per-unit length, the weld height reduces as travel speed increases. As shown in Fig. 15, weld height reduces from 1.9 to 1.3 mm with the increase in travel speed from 250 to 300 mm min^{-1}.

According to Fig. 16 the weld height increases as welding position reduces from 0 to 90°, and then it increases with the further increase in welding position. This trend is due to the trend of C. When the weld bead concavity increases, the weld

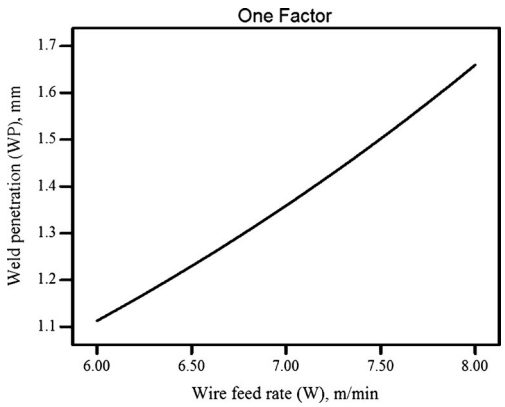

Fig. 9 Direct effect of wire feed rate on weld penetration

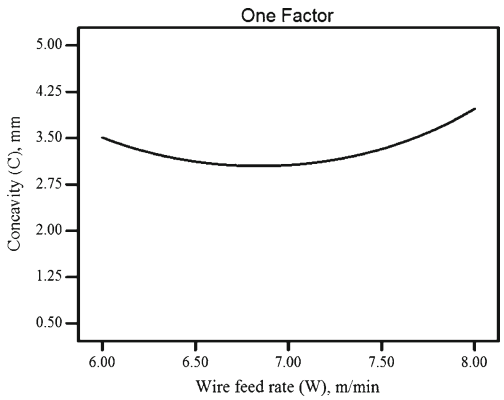

Fig. 11 Direct effect of wire feed rate on concavity

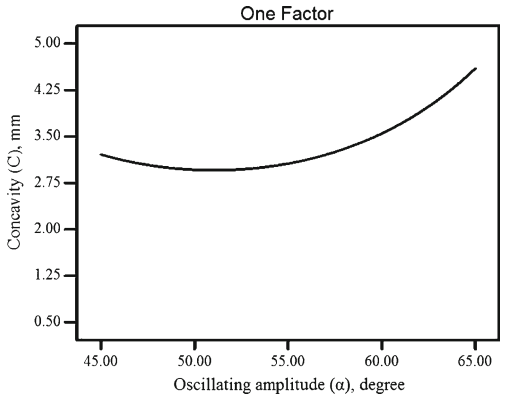

Fig. 12 Direct effect of oscillating amplitude on concavity

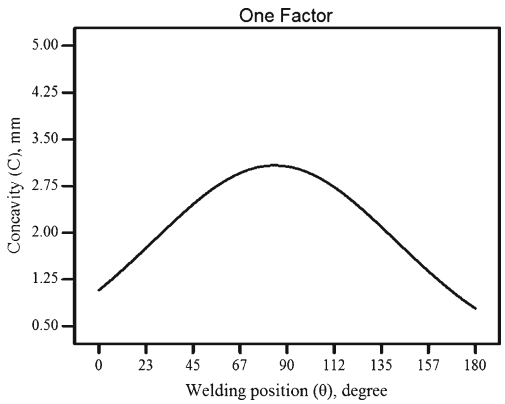

Fig. 13 Direct effect of welding position on concavity

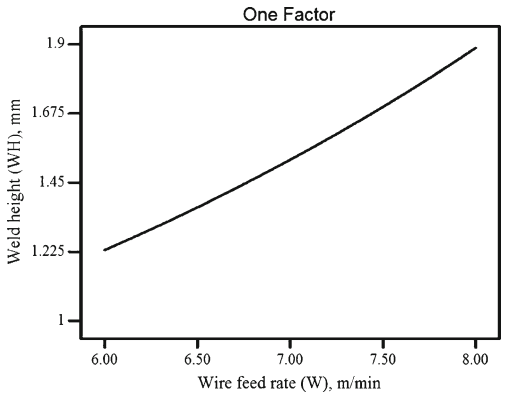

Fig. 14 Direct effect of wire feed rate on weld height

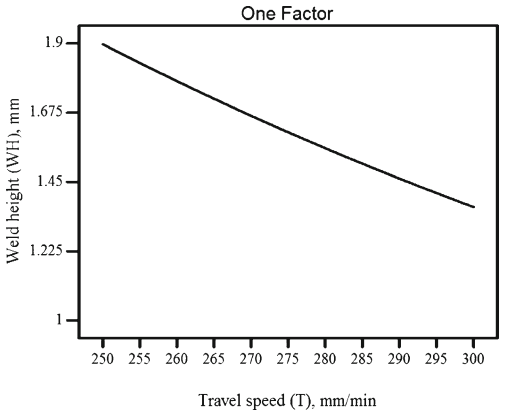

Fig. 15 Direct effect of travel speed on weld height

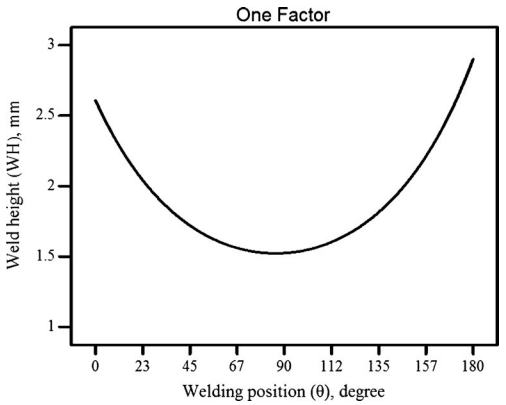

Fig. 16 Direct effect of welding position on weld height

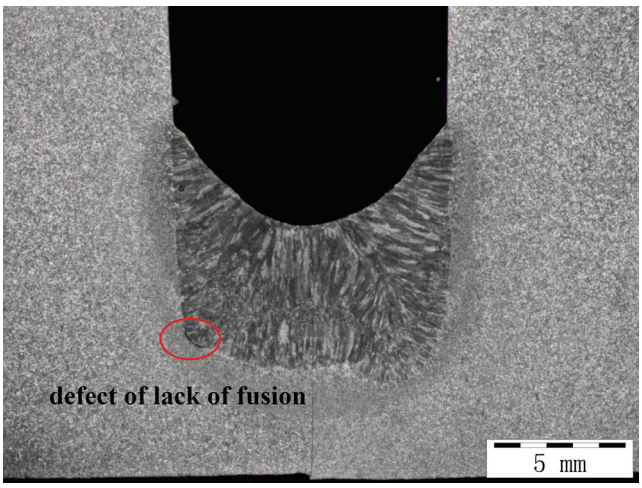

Fig. 17 Defect of lack-of-fusion

Table 9 Constrain of numerical optimization

Name	Goal	Lower	Upper	Importance
W	Is in range	6	8	3
T	Is in range	214	353	3
S	Is in range	100	300	3
α	Is in range	45	65	3
θ	Is equal to	0.00	180.00	3
SP	Maximize	0.19	0.64	5
WP	Maximize	0.90	3.04	5
WH	Maximize	1.03	3.50	3

Table 10 Optimal parameters

W (m min^{-1})	T (mm min^{-1})	S (ms)	α (°)	θ (°)
8	283	200	55	0
7.4	297	158	54	45
7.7	289	300	55	90
7.4	269	242	59	135
8	283	200	55	180

height could decrease with the other weld parameters remaining constant.

5.5 Optimization of the welding parameters by numerical method

Welding defects should be particularly avoided in NG-GMAW because of the great difficulty in repairing NG-GMAW bead. As previously mentioned, NG-GMAW has the high tendency of defect of lack-of-fusion which are shown in Fig. 17. The defect is associated with sidewall penetration and weld penetration according to the experiments. So, maximizing the sidewall penetration and weld penetration is the criterion for optimizing the welding parameters. In order to optimize welding parameters at any position, the welding position can be equal to any value from 0 to 180. Table 9 lists the goal, lower, upper limits as well as the importance for each response and input factors of the criteria. The selected optimal welding parameters at 0, 45, 90 and 135° is shown in Table 10. The weld cross sections with the optimal parameters are shown in Fig. 18.

6 Conclusions

In this paper, the oscillating arc narrow gap all-position GMA welding has been experientially studied and statistically analyzed. The following conclusions are from the present research.

1. RSM based on CCD can be employed to develop a statistical model for predicting weld bead geometry in oscillating arc narrow gap all-position GMA welding.
2. Wire feed rate had a significant positive effect on most of the important weld bead parameters, while travel speed had a negative effect on weld height; oscillating amplitude of arc had a positive effect on the weld bead concavity, and dwell time has a positive effect on sidewall penetration; the welding position was a significant factor for weld bead geometry.

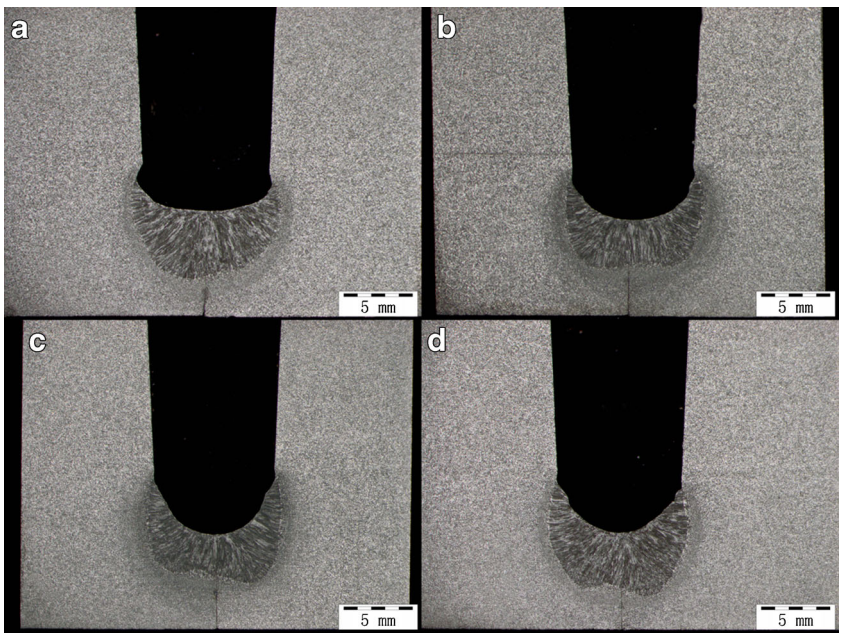

Fig. 18 Cross sections of weld with optimal parameters at different welding positions (**a** 0°; **b** 45°; **c** 90°; **d** 135°)

3. The desired weld bead shape can be achieved by selecting the optimal welding parameters with the developed models, and the model can be employed in automated all-position GMA welding for thick-walled pipes.

Acknowledgments The authors would like to thank the State Key Laboratory of Advanced Welding and Joining of China, all of the work within which were conducted. They also thank the National Natural Science Foundation of China for its financial support (no.51275109).

References

1. Christensen KH, Sørensen T, Kristensen J (2005) Gas metal arc welding of butt joint with varying gap width based on neural networks. Sci Technol Weld Join 10(1):32–43. doi:10.1179/174329305X19303
2. Malin VY (1983) State-of-the-art of narrow gap welding. Weld J 62(Compendex):22–30
3. Wang JY, Ren YS, Yang F, Guo HB (2007) Novel rotation arc system for narrow gap MAG welding. Sci Technol Weld Join 12(6):505–507. doi:10.1179/174329307x213756
4. Murakami S, Kitagawa A, Nakajima H, Nagai A, Yonezawa M (1986) A study on horizontal narrow gap welding for heavy plates. Hitachi Zosen Technol Rev 47(1):33–38
5. Hirakoso K, Kano M, Nomura K (1980) Welding apparatus with shifting magnetic field. U.S Patent 4190760 A, 26 Feb
6. Guo N, Lin SB, Gao C, Fan CL, Yang CL (2009) Study on elimination of interlayer defects in horizontal joints made by rotating arc narrow gap welding. Sci Technol Weld Join 14(6):584. doi:10.1179/136217109X456942
7. Min D, Xin-hua T, Feng-gui L, Shun Y (2010) Welding of quenched and tempered steels with high-spin arc narrow gap MAG system. Int J Adv Manuf Technol 55(5–8):527–533. doi:10.1007/s00170-010-3052-1
8. Wang J, Zhu J, Fu P, Su R, Han W, Yang F (2012) A swing arc system for narrow gap GMA welding. Isij Int 52(1):110–114
9. Xu WH, Lin SB, Fan CL, Yang CL (2012) Feasibility study on tandem narrow gap GMAW of 65 mm thick steel plate. China Weld 21(3):7–11
10. Lassaline E, Zajaczkowski B, North TH (1989) Narrow groove twin-wire GMAW of high-strength steel. Weld J 68(9):53–58
11. Manonmani K, Murugan N, Buvanasekaran G (2007) Effects of process parameters on the bead geometry of laser beam butt welded stainless steel sheets. Int J Adv Manuf Technol 32(11–12):1125–1133. doi:10.1007/s00170-006-0432-7
12. Kim IS, Basu A, Siores E (1996) Mathematical models for control of weld bead penetration in the GMAW process. Int J Adv Manuf Technol 12(6):393–401. doi:10.1007/BF01186927
13. Gunaraj V, Murugan N (1999) Application of response surface methodology for predicting weld bead quality in submerged arc welding of pipes. J Mater Process Technol 88(1):266–275. doi:10.1016/S0924-0136(98)00405-1
14. Koleva E (2005) Electron beam weld parameters and thermal efficiency improvement. Vacuum 77(4):413–421. doi:10.1016/j.vacuum.2004.09.002
15. Starling C, Marques PV, Modenesi PJ (1995) Statistical modelling of narrow-gap GTA welding with magnetic arc oscillation. J Mater Process Technol 51(1):37–49. doi:10.1016/0924-0136(94)01356-6
16. Kim J, Kim I, Lee J, Jung S (2011) An experimental study on the prediction of back-bead geometry in pipeline using the GMA welding process. Int Sci J 49(1):53–61
17. Badkar DS, Pandey KS, Buvanashekaran G (2012) Application of the central composite design in optimization of laser transformation hardening parameters of commercially pure titanium using Nd:YAG laser. Int J Adv Manuf Technol 59(1–4):169–192. doi:10.1007/s00170-011-3492-2
18. Ii EJL, Torres GCF, Felizardo I, Filho FAR, Bracarense AQ (2005) Development of a robot for orbital welding. Ind Robot: Int J 32(4):321–325. doi:10.1108/01439910510600182